

Cobalt-catalysed nucleophilic fluorination in organic carbonates

Susana García-Abellán,^a Daniel Barrena-Espés,^b Julen Munarriz,^b Vincenzo Passarelli^a and Manuel Iglesias^{*,a}

Received 00th January 20xx,
Accepted 00th January 20xx

DOI: 10.1039/x0xx00000x

The novel P-N ligand 1-((diphenylphosphaneyl)methyl)-1H-benzo-1,2,3-triazole (**1**), based on a benzotriazole scaffold, has been prepared. The reaction of **1** with [CoCp*(CH₃CN)₃][BF₄]₂ and [CoCp*(I)₂]₂ (Cp* = pentamethylcyclopentadienyl) affords the chelate complexes [CoCp*(CH₃CN)(P-N)][BF₄]₂ (**2**) and [CoCp*(I)(P-N)]I (**3**), respectively. Complexes **2** and **3** were studied as catalysts in the fluorination of aromatic and aliphatic acyl chlorides in CH₂Cl₂, with **3** showing notably higher activities than **2**. Subsequently, organic carbonates (dimethyl carbonate and propylene carbonate) were also employed as solvents, which led to shorter reaction times and to the broadening of the substrate scope to a variety of aliphatic halides. Comparative studies between **3** and the analogous complex [CoCp*(I)₂(PMePh₂)]I, which features a monodentate phosphane ligand, showed that higher yields were obtained in the case of the former. DFT calculations and experimental studies were performed in order to shed light on the reaction mechanism, which entails the formation of a cobalt fluoride species that reacts via nucleophilic attack with the substrate to afford the corresponding fluorinated compounds.

Introduction

The development of efficient and selective methods for the fluorination of organic molecules has gained increasing importance over the past decades owing to the pivotal role of fluorine-containing compounds in the pharmaceutical and agrochemical industries.¹⁻³ The availability of appropriate fluorination methods that make use of readily available and easy-to-handle reagents is crucial for the progress of synthetic fluorine chemistry. Noteworthy, great advances have been made in electrophilic fluorination methods,⁴⁻⁷ however, “F⁺” sources are expensive and, in some cases, present limited synthetic applications. In this regard, nucleophilic fluorination catalysed by transition metal complexes has received significant interest during the past decade.⁸ This methodology makes use of the broad variety of readily available and inexpensive nucleophilic “F⁻” sources (*e.g.*, metal fluorides). In view of the design of more sustainable processes, the use of new catalysts based on Earth-abundant metals is desirable due to the fact that they are broadly available, inexpensive, and present low toxicity.⁹⁻¹²

Cobalt complexes, in particular, have been successfully employed as catalysts for several nucleophilic fluorination reactions. The enantioselective incorporation of fluorine into epoxides has been described to occur via nucleophilic fluorination by means of Co-salen-type catalyst in the presence of chiral amines, employing benzoyl fluoride and 1,1,1,3,3,3-hexafluoroisopropanol as HF source.^{13,14} The synthesis of acyl fluorides from acyl chlorides has been accomplished by means of cobalt(III) catalysts based on the CoCp* scaffold (Cp* = pentamethylcyclopentadienyl), employing 3 equivalents of AgF as fluoride source.^{15,16} With respect to these kind of processes, more recently, a related piano-stool rhodium complex has been

described to catalyse this transformation and applied to the synthesis of the API probenecid with excess AgF.¹⁷ However, to the best of our knowledge, the substrate scope for these Co- and Rh-Cp* complexes has not been extended beyond acyl chlorides. A single-atom catalysts (SAC) based on cobalt has shown excellent activities in the fluorination of acyl chlorides.¹⁸ The reaction mechanism of Co(III)-catalysed nucleophilic fluorination reactions has not been studied in depth from a theoretical perspective, probably due to the scarcity of this type of processes. Namely, only a qualitative reaction mechanism proposed by Baker and co-workers is available in the literature.^{15,16} According to their proposal, the Co-F complex acts as a source of nucleophilic fluoride in a stepwise process, in which the fluoride undertakes a nucleophilic attack on the carboxylic carbon of the benzoyl chloride reagent. This leads to an anionic [C(O)(R)(Cl)(F)]⁻ reaction intermediate that releases chloride with concomitant formation of a Co(III)-Cl complex. Finally, the initial Co(III)-F active species is recovered by reaction with AgF, which fluorinates the metal centre, producing AgCl. A similar process catalysed by a cyclometallated Rh-Cp* complex has been recently reported. In this case, the authors proposed that the fluorination reaction proceeds *via* a Rh-F species, which directly transfers the fluorine moiety to the carbonyl carbon of the reagent in a concerted process.¹⁷

Herein, we report on the catalytic activity of a series of Co(III)Cp* complexes featuring novel bidentate P-N ligands based on a triazole scaffold, which act as efficient catalysts for the nucleophilic fluorination of a range of substrates, including aromatic and aliphatic acyl chlorides, as well as benzyl halides and alkyl iodides. These catalysts proved to work efficiently in organic carbonates, thus allowing the replacement of chlorinated solvents. Moreover, in order to expand the molecular understanding of these processes, we explored the potential reaction mechanism by means of Density Functional Theory (DFT).

^a Instituto de Síntesis Química y Catálisis Homogénea-ISQCH, Universidad de Zaragoza-C.S.I.C., C/ Pedro Cerbuna 12, Facultad de Ciencias, 50009-Zaragoza, Spain, E-mail: miglesia@unizar.es

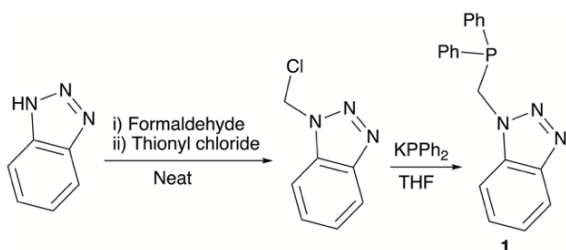
^b Departamento de Química Física y Analítica. Universidad de Oviedo. Avda. Julián Clavería 8, 33006-Oviedo, Spain.

† Electronic Supplementary Information (ESI) available: ¹H NMR data and DFT details. CCDC 2193135.

Results and discussion

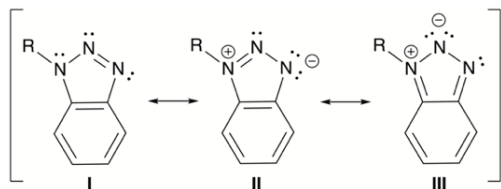
Synthesis of cobalt complexes **2** and **3**.

We prepared a new P-N ligand (1-((diphenylphosphanyl)methyl)-1*H*-benzo-1,2,3-triazole) based on a 1,2,3-triazole scaffold (**1**). This heterotopic ligand may be able to generate a vacant coordination site thanks to the potential hemilabile nature of the triazol moiety, thus enhancing the activity and stability of the catalyst. The synthesis of **1** was achieved in good yields by reaction of (1-chloromethyl)-1*H*-benzo-1,2,3-triazole with KPPH₂ in THF. The synthesis of the chloride intermediate was accomplished by modification of a reported procedure,¹⁹ which entails the reaction of benzotriazole with formaldehyde and thionyl chloride according to a sequential reaction.



Scheme 1. Synthetic route for the preparation of **1**.

The coordination of N1-substituted benzotriazoles is more prone to occur by the N3 than the N2 due to the stronger Lewis basic character of the former. The electronic structure of **1** can be easily visualized by the resonance structures depicted in Scheme 2, which show that the presence of a negative charge at N2 involves the dearomatization of the benzenic ring (III; Scheme 2).²⁰

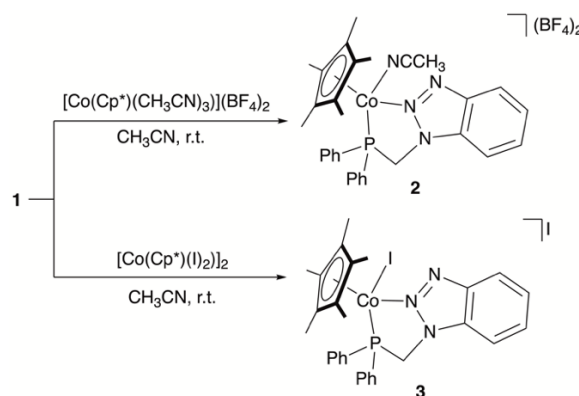


Scheme 2. Resonance structures of **1**.

Therefore, the less favourable N2-coordination would be imposed by the chelate effect. In order to test this explanation, we considered a computational model in which we replaced the *N*-substituent by methyl groups (see Supporting Information, Figure S52). This way, we removed the constraints imposed by the chelate effect, and we coordinated the benzotriazole scaffold by the N2 and N3 nitrogen atoms. As expected, coordination by N3 was 4.9 kcal·mol⁻¹ more favourable than by N2. This result further supports the fact that coordination by N2 is a consequence of the chelate effect.

The reaction of **1** with 1 equivalent of [CoCp*(CH₃CN)₃][BF₄]₂ allows the synthesis of [CoCp*(CH₃CN)(P-N)][BF₄]₂ (**2**) in good yields (see Scheme 3; above). In order to compare the catalytic activity of **2** with a related complex featuring an iodide ligand instead of CH₃CN, we prepared complex **3**, [Co(Cp*)(I)(P-N)]⁺, by

reaction of **1** with 0.5 equivalents of [Co(Cp*)(I)₂]₂ (Scheme 3; below).



Scheme 3. Synthetic route for the preparation of complexes **2** and **3**.

Upon coordination, the phosphorus peak in the ³¹P{¹H} NMR spectrum shifts from δ -17.5 to 62.1 ppm. The ¹H NMR spectrum of complex **2** shows as main diagnostic signals those of the diastereotopic methylenic protons, which appear as an apparent triplet at δ 5.80 ppm (²J_{H-H} = 14.6 Hz) and a doublet of doublets at δ 4.55 ppm (²J_{H-H} = 14.6 and ²J_{H-P} = 1.7 Hz). Note that these methylenic protons come about as a doublet at δ 5.45 ppm (²J_{P-H} = 5.0 Hz) in ¹H NMR spectrum of **1**. Further proof of ligand coordination is the doublet resonance in the ¹³C{¹H} NMR at δ 104.9 ppm (²J_{C-P} = 1.7 Hz) due to the quaternary carbon nuclei of the Cp* ligand.

Single-crystal X-ray diffraction analysis confirms the connectivity proposed for **2** (Figure 1). The cation exhibits a three-legged piano stool geometry with the Cp* ligand coordinating η⁵ to the cobalt centre. The P-N ligand behaves as a chelate, with a N25–Co–P bite angle of 83.43(7)°, which leads to a slightly distorted pseudo-octahedral environment for the cobalt centre, with the remaining coordination site being occupied by an acetonitrile ligand. It is noteworthy that both N25 and N26 atoms of the triazole present a lone pair, which renders two Lewis basic sites at the triazole moiety that may coordinate the Co centre (*vide infra*). Nonetheless, selective bidentate coordination by the P atom and N25 is observed, which eventually leaves a non-bonding pair at N26. The N24–N25 bond length of 1.361(3) Å is in the range of that expected for an aromatic N–N bond, while the N25–N26 bond length (1.294(3) Å) is noticeably shorter, suggesting a double bond character, which agrees with the resonance structure without charge separation (I) depicted in Scheme 2. The ¹H and ¹³C NMR spectra of **3** are similar to those previously described for **2**, showing only slight shifts of the peaks. The most noticeable differences involve the ³¹P{¹H} NMR spectrum, which shows a shift from δ 62.1 ppm in **2** to 59.0 ppm in **3**, and the singlet resonance that corresponds to the Cp* in the ¹H NMR spectrum, which shifts from δ 1.40 to 1.66 ppm for **2** and **3**, respectively.

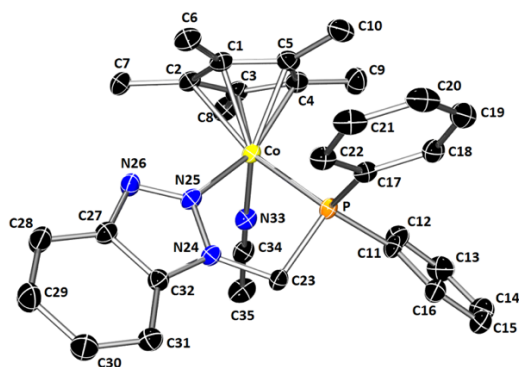


Figure 1. ORTEP view of **2** (ellipsoids are drawn at the 50% probability level). Hydrogen atoms and the BF_4^- counterions are omitted for clarity. Selected bond lengths (Å) and angles (deg): P–Co 2.2331(19), N25–Co 1.968(3), N33–Co 1.923(3), C1–Co 2.086(3), C2–Co 2.106(3), C3–Co 2.109(3), C4–Co 2.076(3), C5–Co 2.104(3), Co–CT 1.7081(11), N24–N25 1.361(3), N25–N26 1.294(3), N24–N25–N26 110.6(2), C32–N24–N25 108.7(2), C32–N24–N23 131.2(2), N25–N24–C23 120.1(2), N25–N26–C27 107.3(2), N26–N25–Co 129.36(18), N24–N25–Co 120.02(18), N25–Co–P 83.43(7), N33–Co–P 90.25(9), CT–Co–P 131.37(4), CT–Co–N33 122.45(8), CT–Co–N25 125.54(8). CT: centroid of C1, C2, C3, C4, and C5.

Initial tests to probe the catalytic activity of complexes **2** and **3** were aimed at exploring the fluorination of benzoyl chloride, employing a 5 mol % catalyst loading and 2.5 eq. of AgF in CH_2Cl_2 at room temperature. Under these conditions, **3** led to a 100 % conversion in 2.5 h, while **2** only reaches a 46% conversion after 5 h. This difference in activity is likely due to a lower concentration of the active species, plausibly a cobalt fluoride complex ($[\text{Co}]\text{-F}$). In the case of **2**, the equilibrium $[\text{Co}]\text{BF}_4 + \text{AgF} \rightleftharpoons [\text{Co}]\text{-F} + \text{AgBF}_4$ takes place, which brings about a low concentration of $[\text{Co}]\text{-F}$ in solution. In contrast, the activation of **3** gives AgI as by-product, which is barely soluble in CH_2Cl_2 , thus favoring the formation of the Co-F species ($[\text{Co}]\text{I} + \text{AgF} \rightarrow [\text{Co}]\text{-F} + \text{AgI}\downarrow$).

Prompted by these results, the activity of **3** was evaluated for a variety of acyl chlorides (Table 1); namely, 4-chlorobenzoyl chloride, 4-methoxybenzoyl chloride, 4-nitrobenzoyl chloride, and isovaleryl chloride. As can be observed in Table 1, for aromatic acyl chlorides, all the reactions reach full conversion before 4.5 h in CH_2Cl_2 at room temperature, but longer reaction times are required in the case of isovaleryl chloride (Entry 5). The use of 1.1 equiv. of AgF results in longer reactions times and, in some cases, lower yields (Entries 2 and 5). Subsequently, we carried out an optimization of the initial conditions using organic carbonates, which are considered green solvents due to their low volatility, good biodegradability and low toxicity.²¹ The use of dimethyl carbonate (DMC) permits an increase of the reaction temperature to 80 °C; however, longer reaction times compared to CH_2Cl_2 are required. It is worth noting that a progressive decrease of the yield is observed at long reaction times for 4-nitrobenzoyl chloride and isovaleryl chloride, which may be attributed to reaction of the acyl fluoride with DMC.

Under analogous conditions, propylene carbonate (PC) leads to quantitative yields in short reaction times (Table 1), significantly improving the results obtained with CH_2Cl_2 and DMC. Interestingly, at prolonged reaction times the initial solution

solidifies, thus suggesting that the polymerization of PC may occur.^{22–24} This behaviour was detected for all the substrates to some degree, but it is more noticeable for isovaleryl chloride (Entries 4 and 5, Table 1), in which case full conversion cannot be achieved. However, the use of PC allows for the straightforward isolation of the fluoride via vacuum distillation (see preparative synthesis of isovaleryl fluoride in the ESI).

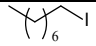
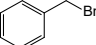
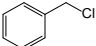
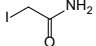
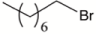
Table 1. Fluorination of acyl chlorides with **3** (5 mol%).

Entry	Substrate	Yields % (time in h) ^[a]			
		$\text{CH}_2\text{Cl}_2^{\text{b}}$		DMC ^c	PC ^c
		2.5 eq. AgF	1.1 eq. AgF		
1		>99 (2.5)	100 (6)	93 (3.5)	>99 (0.25)
2		>99 (2.5)	48 (24)	80 (4)	>99 (0.25)
3		>99 (4.5)	100 (7)	>99 (5)	>99 (0.25)
4		>99 (1.5)	100 (24)	98 (4)	>99 (0.25)
5		96 (24)	46 (24)	>99 (5)	92 (1)

^a Yields calculated by ^{19}F NMR using fluorobenzene as internal standard. ^b Room temperature (2.5 or 1.1 eq. AgF). ^c 80 °C, (2.5 eq. AgF).

Finally, the substrate scope was expanded to aliphatic halides, i.e., 1-iodooctane, benzyl bromide, benzyl chloride and iodoacetamide (Table 2). The conversions in CH_2Cl_2 at room temperature are relatively low except in the case of benzylbromide (Entry 2, Table 2), and long reaction times are required. The use of a high boiling point polar solvent such as DMF led to a 41 % conversion of 1-iodooctane in 4 h at 80 °C, while PC, under analogous conditions, renders quantitative yields after 3 h. The use of benzyl bromide and benzyl chloride as substrates results in lower yields (Entry 2 and 3, Table 2) because PC polymerization is significant before full conversion is achieved. In order to probe the functional group tolerance for this reaction, the fluorination of iodoacetamide was explored, giving rise to quantitative conversions in 1 h (Table 2, Entry 4).[‡]

Table 2. Fluorination of alkyl halides with **3** (5 mol%).

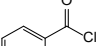
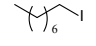
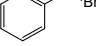
Entry	Substrate	Yields % (time in h) ^[a]		
		CH ₂ Cl ₂ ^b	DMF ^c	PC ^c
1		19 (24)	41 (4)	100 (3)
2		76 (24)	56 (4)	83 (2)
3		0 (24)	11 (4)	53 (4)
4		-	-	100 (1)
5		-	-	3 (3)

^a Yields calculated by ¹⁹F NMR using fluorobenzene as internal standard. ^b Room temperature (2.5 eq. AgF). ^c 80 °C (2.5 eq. AgF).

The reaction with a 1-bromoalkane; namely, 1-bromooctane, was evaluated in PC at 80 °C, resulting in very low conversions (Table 2, Entry 5).

In order to evaluate the influence of the triazol moiety in **3**, we explored the activity of the related complex [CoCp*(I)₂(PMePh₂)]I in a series of representative reactions. In all cases, **3** leads to better yields than [CoCp*(I)₂(PMePh₂)]I under the same reaction conditions. This effect is especially noticeable in the case of 1-iodooctane (Table 3, Entry 2 and Table 3, Entry 1), plausibly due to the fact that the stabilizing effect of the triazol moiety becomes more significant under harsher conditions.

Table 3. Fluorination of alkyl halides with CoCp*(I)₂(PMePh₂)]I (5 mol%).

Entry	Substrate	Solvent	Yields % (time in h) ^[a]
1 ^[b]		CH ₂ Cl ₂	91 (2.5)
3 ^[c]		PC	41 (3)
4 ^[c]		PC	70 (2)

^a Yields calculated by ¹⁹F NMR using fluorobenzene as internal standard. ^b Room temperature (2.5 eq. AgF). ^c 80 °C (2.5 eq. AgF).

Finally, the fact that the reactions are carried out in a polar aprotic media, i.e., organic carbonate solvents, and the fluoride is a strong nucleophile, prompted us to verify whether direct substitution without the catalyst could take place. Therefore, the reactions of NaF or AgF with benzoyl chloride and iodoctane was explored in the absence of the Co catalyst in PC under otherwise analogous conditions to those described above. No conversion was observed with NaF, and, in the case of AgF, yields below 30% were observed, even at long reaction times.

To better understand the reaction mechanism of Co(III)-based nucleophilic fluorination, we performed a DFT-based study of the reaction mechanism. In this regard, we note that, as it will be shown below, all the intermediates and transitions states

bear a Co(III) in a pseudo-octahedral saturated coordination environment, with a *d*⁶ valence electron configuration that is generally considered to be in the singlet low-spin configuration. Nonetheless, there are some examples reported in the literature in which higher spin states of octahedral Co(III) complexes are found to be relevant,²⁵⁻³⁰ in general, in lower coordination environments.³¹⁻³⁶ Even so, the possibility of the Co(III) catalysts being in the triplet state, which could open the door to multi-state reactivity,^{37,38} has been generally overlooked in the literature, with very few exceptions, especially when considering octahedral coordination environments.^{39,40,41}

In this context, in order to select a method suitable for both, energy barriers and spin states, we considered a series of exchange-correlation functionals, which include pure functionals: M06-L⁴² and TPSS,⁴³ as well as hybrid ones: M06,⁴⁴ B3LYP,^{45,46} and TPSSH.^{47,48} The method selection was made on the following basis: TPSS and TPSSH have been ranked in the top of several benchmark studies on the spin state of Co complexes,^{39,49} in addition, TPSSH has also been applied to describe the spin state of a dinuclear Co-catalyst for the semireduction of alkynes,⁵⁰ and TPSS has been applied to C–H bond activation by cobalt-imido complexes.⁵¹ This way, even though they are not commonly employed for chemical reactivity, they are valuable to explore the possibility of Co(III)-triplet state structures. M06-L has also been shown to perform reasonably well in predicting the spin state of Co complexes,^{39,49} and has demonstrated a good performance on catalytic studies of related systems.⁵²⁻⁵⁴ M06 and B3LYP are hybrid functionals very commonly used in catalysis, and have also been applied to related processes.^{40,55-58} The Gibbs energy results for the reaction mechanism of the Co-F assisted nucleophilic fluorination reaction of benzoyl chloride (*vide infra*) are provided in Table S2, and, as somehow expected, there is a relatively big dispersion in the results, B3LYP and M06-L providing similar activation barriers (15.3 and 16.7 kcal·mol⁻¹, respectively), while M06 predicts an intermediate value (23.7 kcal·mol⁻¹), and TPSS and TPSSH provide the highest one (29.1 and 30.7 kcal·mol⁻¹, respectively). The electronic and Gibbs energy difference between singlet and triplet states is shown in Table S3.⁵ As can be seen in all cases, the singlet state is the most stable spin state, although the singlet-triplet gap is strongly dependent on the functional. Namely, TPSS and M06-L predict an electronic energy difference between the singlet and the triplet state higher than 12 kcal·mol⁻¹ in all cases. This difference decreases for TPSSH, which correlates with the well-known over-stabilization of high spin states characteristic of hybrid functionals. In this line, the singlet-triplet gap keeps decreasing when M06 and B3LYP are considered, the singlet state being about 5 kcal·mol⁻¹ more stable for B3LYP and 4 kcal·mol⁻¹ for M06. The effect is more pronounced when Gibbs energies are taken into account, both systems having very close stabilities in some cases. Nonetheless, both functionals (M06 and B3LYP) have been ranked as poor performers in predicting the spin state of Co(III) complexes,³⁸ and were thus discarded. On the other hand, TPSSH has been shown to be the best hybrid functional for predicting the spin state of Co(III) complexes,³⁹

and TPSS and M06-L have, as previously explained, also been shown to exhibit a good performance in this task.^{39,49} Therefore, we are confident that all the structures involved in the reaction pathways correspond to Co(III) low spin singlet states. Moreover, in operando ³¹P NMR, spectra show exclusively the presence of **3**. This way, given its reported good performance in the study of reaction mechanisms,⁵²⁻⁵⁴ we consider the M06-L functional for the proposal and discussion of the reaction mechanism.

A previous study proposed that the first step entails the substitution of the iodido ligand by a fluoride.^{16,17} Therefore, we considered an analogous first step for our reaction. Subsequently, given the potential lability of the triazol moiety of the P-N ligand, its substitution by a second fluoride would render the difluoride species **A_{Co-F}**, which we propose as the active species (see Figure 2a). Note that the Co-F subindex highlights the fact that this species bears a Co-F bond that is active in nucleophilic fluorination reactions. DFT calculations point towards the reaction proceeding by means of a concerted nucleophilic fluorine attack at the carbonyl carbon of the acyl

chloride, via **TS_{A-B}** (see Figure 2b). This process is affordable from an energetic point of view, as it bears a Gibbs energy barrier of 16.6 kcal·mol⁻¹, and directly leads to the acyl fluoride and the formation of intermediate **B_{Co-Cl}**, which is 16.8 kcal·mol⁻¹ more stable than **A_{Co-F}**. Then, we expect that the chlorido ligand in **B_{Co-Cl}** will be substituted by a fluoride anion via reaction with AgF, producing AgCl as by-product. Note that the energy barrier of this process is very similar to that recently reported for a Rh-catalysed nucleophilic fluorination reaction (16.6 vs 16.7 kcal·mol⁻¹).¹⁷ In this regard, we also explored a stepwise reaction mechanism, in which the fluoride anion is transferred first, leading to an anionic quaternary intermediate [C(O)(Cl)(F)(R)]⁻, similar to that proposed by Baker *et al.*¹⁵ Nevertheless, we could not locate either the transition state or the intermediate on the Potential Energy Surface. On the contrary, we found an alternative reaction pathway in which the fluoride-chloride exchange takes place by means of a sigma-bond metathesis. However, the associated transition state (**TS_{A-B-meta}** in Figure S53) was 30.2 kcal·mol⁻¹ higher in Gibbs energy than **TS_{A-B}**, and was thus discarded.

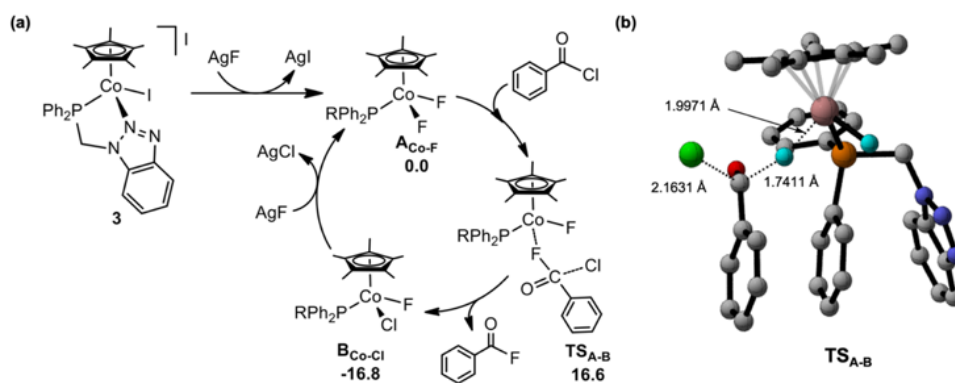


Figure 2. (a) Proposed catalytic cycle for the **3**-catalyzed nucleophilic fluorination reaction and the basis of DFT calculations (R = 1-methylenebenzoimidazole). Gibbs energies are expressed in kcal·mol⁻¹, and are calculated with respect to **A_{Co-F}** and isolated molecules. (b) DFT-optimized structures for transition structure **TS_{A-B}**; hydrogen atoms have been omitted for clarity

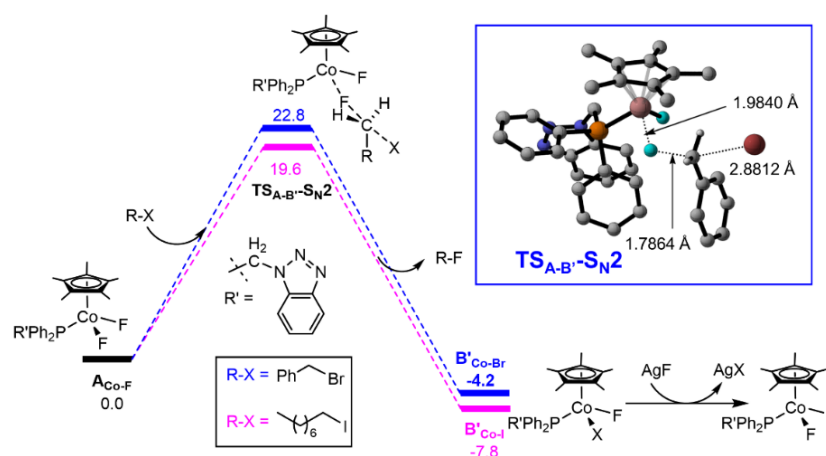


Figure 3. DFT-computed reaction profile for the Co-F assisted S_N2 fluorination reaction of benzyl bromide (blue) and 1-iodooctane (pink). Energy values are provided in kcal·mol⁻¹ and calculated with respect to **A_{Co-F}** and isolated molecules. The geometrical structure of **TS_{A-B-SN2}** for benzyl bromide substrate is shown in the insert; note that non-relevant hydrogen atoms have been omitted for clarity.

Encouraged by these results, we extended the mechanistic exploration to the fluorination of aliphatic halides. Namely, we considered benzyl bromide and 1-iodooctane as substrates (see Table 2). The calculations suggest that the reaction proceeds via an S_N2 reaction mechanism assisted by the Co–F bond (see Figure 3). For the sake of clarity, we refer to the transition structure as $TS_{A-B}-S_N2$ (shown in Figure 3 for benzyl bromide and in Figure S54 for 1-iodooctane), which shows the Y-shaped carbon atom characteristic of S_N2 reactions. It is remarkable that the Gibbs energy barrier for this process is higher than that obtained for the nucleophilic fluorination of acyl chloride, *i.e.*, 22.8 kcal·mol⁻¹ for benzyl bromide and 19.6 kcal·mol⁻¹ for 1-iodooctane, 6.2 and 3.0 kcal·mol⁻¹ higher than that obtained for TS_{A-B} , respectively. This result is in agreement with the lower reaction rates experimentally observed for the latter substrates in comparison with acyl chlorides. In order to find support for the proposed mechanism, the initial TOF was calculated for various *p*-substituted acyl chlorides with electron-withdrawing and electron-donating groups. The presence of an electron-withdrawing group gives rise to a more electrophilic carbonyl carbon, which should lead to an increase of the initial TOF if the reaction operates by an S_N2 mechanism. The opposite effect is expected for electron-donating groups. The initial TOF values calculated for X = OCH₃, H and NO₂ at 5 min are 14.4, 40.8 and 62.4 h⁻¹, respectively. The kinetic profiles of the reactions are shown in Figure 4a, while the TOF vs ν_{CO} (cm⁻¹) plot is displayed in Figure 4b. In the case of the latter, a linear relationship is observed between the carbonyl vibration frequency of the different acyl chlorides—which is proportionally related with the electrophilicity of the carbon atom—and their corresponding TOF values.

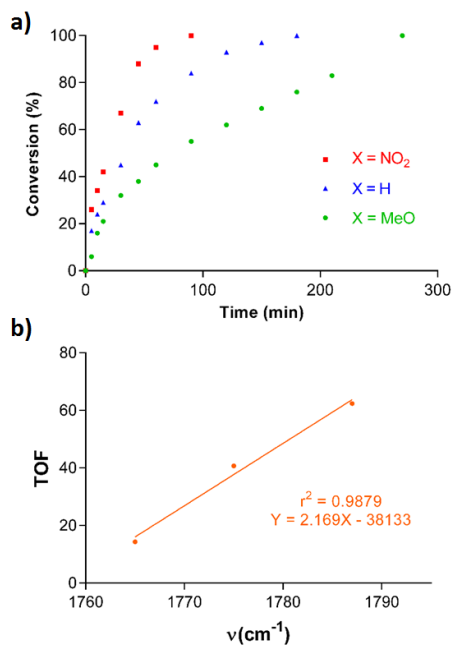


Figure 4. a) Kinetic profiles for the fluorination of acyl chlorides (X = OCH₃, H and NO₂); b) ν_{CO} (cm⁻¹) vs TOF plot.

The experimental activation energy (E_a) for the fluorination of 1-iodooctane in PC employing **3** as catalyst was calculated using the initial reaction rates measured at 60, 80, 100, and 120 °C to afford a value of 16.2 ± 0.5 kcal mol⁻¹ (Figure 5).

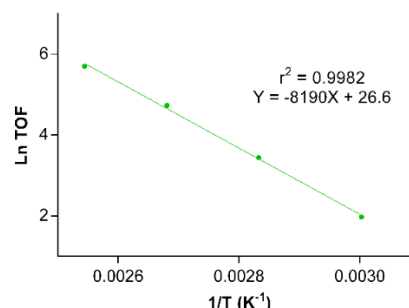


Figure 5. Arrhenius plot for the fluorination of 1-iodooctane with a 5 mol% of **3** in propylenecarbonate.

The experimental E_a agrees well with that obtained by theoretical calculations (19.6 kcal mol⁻¹). Note that the relatively small deviation between the experimental and theoretical values can be attributed to the fact that the former was obtained from reactions performed in PC, while the latter was calculated considering CH₂Cl₂ as the solvent (in the framework of the implicit SMD solvation model).⁵⁹ In this regard, non-protic polar solvents are known to promote S_N2 reactions; thus, the fluorination reaction is expected to be favoured in PC due to its higher polarity—the molecular dipole moment of PC is 4.9 D while that of CH₂Cl₂ is 1.7 D. Note that the dipole moment of DMC is 0.9 D, which accounts for the lower rates observed in this solvent relative to PC, despite the fact that the reaction temperatures are the same. To obtain further support for the S_N2 mechanism, we studied the fluorination of a secondary iodide (iodocyclohexane), which results in no conversion under the conditions described above for the fluorination of 1-iodooctane in PC (Table 1; Entry 1). The stark difference between the reactivity of the primary and secondary alkyl iodide agrees with an S_N2 mechanism.

Finally, complex **3** was reacted with excess AgF (12 equivalents) in CD₂Cl₂. The ¹H NMR spectrum shows that the characteristic resonances of the diastereotopic methylenic protons in **3** disappear to give rise to a doublet at δ 5.71 ppm ($^2J_{H-P} = 5.7$ Hz), as expected for the P-bound ligand with a dangling triazole. In the ³¹P{¹H} NMR spectrum, a new peak emerges at δ 25.1 ppm while the peak of **3** at δ 62.1 ppm disappears. These data point to the dissociation of the triazole moiety due to the coordination of two fluoride ligands. It must be noted that Baker et al. reported a broad signal in the ¹⁹F NMR spectrum at around -710 to -760 ppm for a related complex;¹⁶ however, we were not able to detect the ¹⁹F NMR signal expected for two fluoride ligands, perhaps due to a large peak width.

Conclusions

We have developed a straightforward method for the synthesis of a novel P-N ligand based on a benzotriazole scaffold. The coordination chemistry of this ligand was explored with Co(III)Cp* precursors, i.e., [CoCp*(CH₃CN)₃][BF₄]₂ and [CoCp*(I)₂]₂, which led to the preparation of complexes **2** and **3**, respectively. Complex **3** shows good catalytic activities in the nucleophilic fluorination of aromatic and aliphatic acyl chlorides in CH₂Cl₂. However, **2** was found to perform markedly worse, plausibly due to the lower concentration of the active species in solution due to the equilibrium [Co]BF₄ + AgF ⇌ [Co]-F + AgBF₄, which highlights the importance of the choice of counter anion in these processes. Moreover, the use of **3** as catalyst leads to improved yields compared to the related complex [CoCp*(I)₂(PMePh₂)], especially for substrates that require harsher reaction conditions. This behaviour might be ascribed to the higher stability conferred by the hemilabile triazol moiety.

The use of organic carbonates as solvents, namely, DMC and PC, allowed not only the substitution of a chlorinated solvent by a more sustainable alternative, but also the expansion of the substrate scope to aliphatic halides. Moreover, the use of PC as solvent proved to bring about shorter reaction times and better yields. DFT calculations and experimental data suggest that the reaction mechanism entails the formation of a cobalt fluoride species that reacts via a nucleophilic attack at the acyl chloride or alkyl halide to render the fluorinated compound, with all Co(III)-species involved in the reaction mechanism being in the low-spin singlet state.

Experimental

General information. All experiments were carried out under an inert atmosphere using the Schlenk technique. The complexes were stored under an inert atmosphere or in a MBraun dry box. The solvents were previously dried and distilled under argon or by means of a solvent purification system (SPS) and collected in an inert atmosphere. All other commercially available starting materials were purchased from Sigma-Aldrich and Acros Organics and were used without further purification. The NMR spectra were recorded at 298 K in the Bruker Avance 300 MHz, Bruker ARX 300 MHz and Bruker Avance 400 MHz spectrometers. Chemical shifts are expressed in ppm and the residual peaks of the solvent were taken as reference. Coupling constants *J* are given in Hz. Spectral assignments were achieved by combination of ¹H-¹H COSY, ¹³C APT, ¹H-¹³C HSQC and ¹H-¹³C HMBC experiments. 1-(chloromethyl)-1*H*-benzo-1,2,3-triazole was synthesized according to a preparation previously described in literature.¹⁸ Complexes [Co(Cp*)₂]₂ was synthesized from Co₂(CO)₈ using a synthetic route reported in the literature.⁶⁰

Synthesis of 1-((diphenylphosphanyl)methyl)-1*H*-benzo-1,2,3-triazole (1**).** ^tBuOK (338 mg, 3.00 mmol) was added to a solution of HPPH₂ (524 μL, 3.00 mmol) in dry tetrahydrofuran (10 mL) and was stirred for 2 hours, acquiring a reddish colour. Subsequently, this solution was added dropwise to a solution of 1-(chloromethyl)-1*H*-benzo-1,2,3-triazole (504 mg, 3.00 mmol) in dry tetrahydrofuran (10 mL) by cannula. The solution was

stirred for 1 day. The mixture thus obtained was evaporated under reduced pressure, the precipitate was dissolved in dichloromethane and filtered through celite®, the solvent was evaporated under vacuum and the resulting beige oil was washed with diethyl ether (3 x 15 mL) to afford a yellowish powder corresponding to complex **1** (567 mg, 1.79 mmol, yield = 60 %). ¹H NMR (CD₃CN, 400 MHz): δ 7.96-7.91 (m, 1H, CH_{Ar}), 7.63-7.58 (m, 1H, CH_{Ar}), 7.52-7.47 (m, 4H, CH_{Ar}), 7.46-7.41 (m, 1H, CH_{Ar}), 7.40-7.32 (m, 7H, CH_{Ar}+PCH_{Ar}), 5.45 (d, ²J_{P-H} = 5.0, 2H, CH₂P). ¹³C{¹H} NMR APT, ¹H-¹³C HSQC, ¹H-¹³C HMBC (CD₃CN, 101 MHz): δ 146.7 (s, C_{ipso}N), 136.4 (d, ¹J_{P-C} = 13.2, C_{ipso}P), 134.2 (s, C_{ipso}N), 134.0 (d, ²J_{P-C} = 19.7, C_{Ar-orto}P), 130.6 (s, C_{Ar-para}P), 129.8 (d, ³J_{P-C} = 7.0, C_{Ar-meta}P), 128.0 (s, C_{Ar}N), 124.9 (s, C_{Ar}N), 120.2 (s, C_{Ar}N), 111.7 (d, ⁴J_{P-C} = 3.6, C_{Ar}N), 48.6 (d, ¹J_{P-C} = 17.3, CH₂P). ³¹P{¹H} NMR (CD₃CN, 162 MHz): δ -17.5 (s, PPH₂). HRMS (ESI) Calcd for [M+Na]⁺ 340.0974, found 340.0967.

Synthesis of **2:** The complex [CoCp*₂]₂ (145 mg, 0.31 mmol) was dissolved in acetonitrile (10 mL), AgBF₄ (131 mg, 0.67 mmol) were added and was stirred for 2 hours protected from light. The mixture was filtered through celite®, the solvent was evaporated under reduced pressure and the resulting purple oil was washed with diethyl ether (3 x 15 mL), obtaining the complex [CoCp*(CH₃CN)₃][BF₄]₂. Subsequently, the cobalt complex was dissolved in acetonitrile, 1-((diphenylphosphanyl)methyl)-1*H*-benzo-1,2,3-triazole (194 mg, 0.61 mmol) was added and the solution was stirred for 1 day. The mixture thus obtained was evaporated under reduced pressure and the resulting red powder was washed with diethyl ether (3 x 15 mL) obtaining the corresponding complex **2** (275 mg, 0.38 mmol, yield = 62 %). ¹H NMR (CD₃CN, 400 MHz): δ 8.34-8.28 (m, 1H, CH_{Ar}), 7.94-7.88 (m, 3H, CH_{Ar}), 7.87-7.80 (m, 4H, CH_{Ar}+PCH_{Ar}), 7.73-7.66 (m, 2H, CH_{Ar}+PCH_{Ar}), 7.57-7.52 (m, 2H, PCH_{Ar}), 7.30-7.23 (m, 2H, PCH_{Ar}), 5.80 (at, ²J = 14.6, 1H, CH₂P), 4.55 (dd, ²J_{H-H} = 14.6, ²J_{P-H} = 1.7, 1H, CH₂P), 1.40 (d, ⁴J_{P-H} = 2.7, 15H, C₅(CH₃)₅). ¹³C{¹H} NMR APT, ¹H-¹³C HSQC, ¹H-¹³C HMBC (CD₃CN, 101 MHz): δ 149.8 (s, C_{ipso}N), 136.8 (s, C_{ipso}N), 135.8 (d, ²J_{P-C} = 11.1, C_{Ar-orto}P), 135.2 (d, ⁴J_{P-C} = 2.8, C_{Ar-para}P), 134.4 (d, ⁴J_{P-C} = 3.3, C_{Ar-para}P), 133.5 (d, ²J_{P-C} = 10.3, C_{Ar-orto}P), 132.1 (s, C_{Ar}N), 131.5 (d, ³J_{P-C} = 11.2, C_{Ar-meta}P), 130.9 (d, ³J_{P-C} = 11.4, C_{Ar-meta}P), 128.0 (s, C_{Ar}N), 127.3 (d, ¹J_{P-C} = 47.2, C_{ipso}P), 122.4 (d, ¹J_{P-C} = 52.5, C_{ipso}P), 120.6 (s, C_{Ar}N), 112.2 (s, C_{Ar}N), 104.9 (d, ²J_{P-C} = 1.7, C₅(CH₃)₅), 49.6 (d, ¹J_{P-C} = 30.6, CH₂P), 10.4 (s, C₅(CH₃)₅). ³¹P{¹H} NMR (CD₃CN, 162 MHz): δ 62.1 (bs, PPH₂). ¹⁹F NMR (CD₃CN, 376 MHz): δ -151.4 (s, BF₄). HRMS (ESI) Calcd for [M-CH₃CN]²⁺ 255.5797, found 255.5828.

Synthesis of **3:** The complex [CoCp*₂]₂ (100 mg, 0.11 mmol) was dissolved in dichloromethane (10 mL), 1-((diphenylphosphanyl)methyl)-1*H*-benzo-1,2,3-triazole (71 mg, 0.22 mmol) was added and stirred for 1 day. The solution, previously dark green, turned to dark brown. The solvent was evaporated under reduced pressure, and the resulting brown oil was washed with diethyl ether (3 x 15 mL) to afford the title compound as a redish powder (113 mg, 0.15 mmol, yield = 67%). ¹H NMR (CD₃CN, 400 MHz): δ 8.20-8.15 (m, 1H, CH_{Ar}), 7.99-7.93 (m, 2H, PCH_{Ar}), 7.80-7.76 (m, 1H, PCH_{Ar}), 7.70-7.67 (m, 3H, CH_{Ar}+PCH_{Ar}), 7.61-7.56 (m, 3H, CH_{Ar}+PCH_{Ar}), 7.46-7.41 (m, 2H, PCH_{Ar}), 7.13-7.06 (m, 2H, PCH_{Ar}), 5.76 (at, ²J_{H-H} = 13.6, 1H,

CH₂P), 4.50 (dd, ²J_{H-H} = 13.6, ²J_{P-H} = 2.3, 1H, CH₂P), 1.66 (d, ⁴J_{P-H} = 2.4, 15H, C₅(CH₃)₅). ¹³C{¹H} NMR APT, ¹H-¹³C HSQC, ¹H-¹³C HMBC (CD₃CN, 101 MHz): δ 149.4 (s, C_{ipso}N), 137.1 (d, J_{P-C} = 9.9, C_{Ar}P), 135.3 (d, ³J_{P-C} = 4.8, C_{ipso}N), 134.1 (d, J_{P-C} = 2.8, C_{Ar}P), 133.2 (d, J_{P-C} = 2.8, C_{Ar}P), 133.0 (d, J_{P-C} = 9.6, C_{Ar}P), 131.4 (d, ¹J_{P-C} = 39.9, C_{ipso}P), 131.2 (s, C_{Ar}N), 130.4 (d, J_{P-C} = 9.9, C_{Ar}N), 130.3 (d, J_{P-C} = 11.0, C_{Ar}P), 127.2 (s, C_{Ar}N), 126.1 (d, ²J_{P-C} = 58.0, C_{ipso}P), 119.8 (s, C_{Ar}N), 111.6 (s, C_{Ar}N), 100.7 (d, ²J_{P-C} = 2.2, C₅(CH₃)₅), 52.9 (d, ¹J_{P-C} = 35.6, CH₂P), 11.4 (s, C₅(CH₃)₅). ³¹P{¹H} NMR (CD₃CN, 162 MHz): δ 59.0 (bs, PPh₂). HRMS (ESI) Calcd for [M]⁺ 638.0638, found 638.0642.

General protocol for the fluorination of acyl chlorides. A glass vial was charged with a magnetic stirring bar and the cobalt catalyst (0.006 mmol). Subsequently, the substrate (0.125 mmol), fluorobenzene (12 μL, 0.125 mmol), as internal standard, and 1 mL of solvent were added. AgF (40 mg, 0.312 mmol) was added and the reaction vessel covered with aluminium foil. The reaction mixture was heated if required and samples were taken at given times to monitor the evolution of the reaction by ¹⁹F NMR. The NMR spectra are consistent with literature data.⁶¹ Isovaleryl fluoride has been isolated and characterized (see ESI).

Computational Details. DFT calculations were carried out by using the Gaussian09 suite, revision D.01.⁶² The def2-SVP basis set was used for geometry optimizations and frequency calculations, and electronic energies were further refined via single point calculations with the triple-zeta def2-TZVP basis set.⁶³ The “ultrafine” grid was used in all the calculations (optimizations and single points). For the calculations performed with B3LYP, we included D3BJ dispersion correction scheme⁶⁴ in both, energies and gradient calculations. Note that we did not include additional dispersion corrections in TPSS and TPSSh because we intended to use them for assessing the singlet-triplet gap (which we expect not to be highly influenced by this effect) rather than for computing reaction barriers. Solvent corrections were also included in energies and gradient calculations; we considered the Polarizable Continuum Model (PCM) for B3LYP, TPSSh and TPSS calculations⁶⁵ and the Solvation Model Based on Density (SMD) for M06-L and M06 functionals.⁶⁶ The nature of the stationary points was confirmed by analytical frequency analysis, which was also applied for the calculation of Gibbs energy corrections (at 298.15 K and considering a reference concentration of 1 M). Note that Gibbs energy corrections were calculated at the def2SVP level of theory. For M06-L, B3LYP, TPSSh and TPSS calculations, all structures were optimized by means of the same functional, while for the calculations performed by M06 functional, we considered the M06-L optimized geometry (and thus Gibbs energy corrections), as proposed by other authors.⁵⁸ CylView software was used for structure graphical representations.⁶⁷

Crystal Structure Determination. Single crystals of **2** were obtained by slow diffusion of Et₂O into a solution of **2** in CH₃CN. X-ray diffraction data were collected at 100(2) K on a D8 VENTURE Bruker diffractometers with graphite-monochromated Mo-Kα radiation (λ = 0.71073 Å) using ω-scans and φ-scans. Intensities were integrated and corrected for absorption effects with SAINT-PLUS⁶⁸ and SADABS⁶⁹ programs,

both included in APEX4 package. The structures were solved by the Patterson method with SHELXS-97⁷⁰ and refined by full matrix least-squares on F² with SHELXL-2014⁷¹ under the WinGX suite.⁷²

Crystal data and structure refinement for 2. C₃₁H₃₄B₂CoF₈N₄P, 726.14 g mol⁻¹, triclinic, P-1, a = 10.305(9) Å, b = 11.359(8) Å, c = 14.280(13) Å, α = 92.49(2)°, β = 100.62(3)°, γ = 99.13(2)°, V = 1618(2) Å³, Z = 2, D_{calc} = 1.491 g cm⁻³, μ = 0.655 mm⁻¹, F(000) = 744, prism, 0.40 x 0.20 x 0.14 mm, θ_{min}/θ_{max} 2.040/28.470°, index ranges -13≤h≤13, -15≤k≤13, -19≤l≤19, reflections collected/independent 28506/7904 [R(int) = 0.0447], T_{max}/T_{min} 0.7457/0.5654, data/restraints/parameters 7904/0/430, GooF(F²) = 1.054, R₁ = 0.0602 [I > 2σ(I)], wR₂ = 0.1618 (all data), largest diff. peak/hole 1.560/-0.962 e-Å⁻³. CCDC deposition number 2193135.

Conflicts of interest

There are no conflicts to declare.

Acknowledgements

Grants RTI2018-099136-A-I00 and PID2021-122763NB-I00 funded by MCIN/AEI/10.13039/501100011033 and by “ERDF A way of making Europe”, as well as the “Departamento de Ciencia, Universidad y Sociedad del Conocimiento del Gobierno de Aragón” (group E42_20R) and “Fundación para el Fomento en Asturias de la Investigación Científica Aplicada y Tecnológica” (grant IDI-2021-000054) are gratefully acknowledged. Authors would like to acknowledge the use of *Servicio General de Apoyo a la Investigación-SAI* at the Universidad de Zaragoza and at the ISQCH/CEQMA (CSIC). J.M. acknowledges Dr. Carlos Martín-Fernández and Prof. Victor Polo for fruitful scientific discussions.

Notes and references

‡ Fluoroacetamide is very toxic to human and animal health and must be handled with caution.

§ Note that we also considered the possibility of an open shell singlet configuration for the intermediates and transition state (at the M06-L level), which in all cases converged to the closed shell (singlet) configuration.

- 1 a) United States Food and Drug Administration Advancing Health Through Innovation: New Drug Therapy Approvals 2020; United States Food and Drug Administration: Silver Springs, MD, 2021
- 2 D. E. Yerien, S. Bonesi and A. Postigo, *Org. Biomol. Chem.*, 2016, **14**, 8398–8427.
- 3 c) P. Jeschke, *ChemBioChem*, 2004, **5**, 570–589.
- 4 J.-A. Ma and D. Cahard, *Chem. Rev.*, 2008, **108**, PR1–PR43.
- 5 S. Lectard, Y. Hamashima and M. Sodeoka, *Adv. Synth. Catal.*, 2010, **352**, 2708–2732.
- 6 U. Hennecke, *Angew. Chem. Int. Ed.*, 2012, **51**, 4532–4534.
- 7 S. Lee and W.-j. Chung, *Bull. Korean Chem. Soc.*, 2022, **43**, 896–911.
- 8 C. Hollingworth and V. Gouverneur, *Chem. Commun.*, 2012, **48**, 2929–2942.
- 9 R. M. Bullock, J. G. Chen, L. Gagliardi, P. J. Chirik, O. K. Farha, C. H. Hendon, C. W. Jones, J. A. Keith, J. Klosin, S. D. Minter,

- R. H. Morris, A. T. Radosevich, T. B. Rauchfuss, N. A. Strotman, A. Vojvodic, T. R. Ward, J. Y. Yang and Y. Surendranath, *Science*, 2020, **369**, eabc3183.
- 10 M. Albrecht, R. Bedford and B. Plietker, *Organometallics*, 2014, **33**, 5619–5621.
 - 11 P. Chirik and R. Morris, *Acc. Chem. Res.*, 2015, **48**, 2495.
 - 12 M. Beller, *Chem. Rev.*, 2019, **119**, 2089.
 - 13 J. A. Kalow and A. G. Doyle, *J. Am. Chem. Soc.*, 2010, **132**, 3268–3269.
 - 14 J. A. Kalow and A. G. Doyle, *J. Am. Chem. Soc.*, 2011, **133**, 16001–16012.
 - 15 G. M. Lee, R. Clément and R. T. Baker, *Catal. Sci. Technol.*, 2017, **7**, 4996–5003.
 - 16 M. C. Leclerc, J. M. Bayne, G. M. Lee, S. I. Gorelsky, M. Vasiliu, I. Korobkov, D. J. Harrison, D. A. Dixon and R. T. Baker, *J. Am. Chem. Soc.*, 2015, **137**, 16064–16073.
 - 17 P. J. Morgan, G. C. Saunders, S. A. Macgregor, A. C. Marr and P. Licence, *Organometallics*, 2022, **41**, 883–891.
 - 18 W.-H. Li, B.-C. Ye, J. Yang, Y. Wang, C.-J. Yang, Y.-M. Pan, H.-T. Tang, D. Wang and Y. Li, *Angew. Chem. Int. Ed.* 2022, **61**, e2022097.
 - 19 N. Lebouvier, F. Pagniez, Y. Min Na, D. Shi, P. Pinson, M. Marchivie, J. Guillon, T. Hakki, R. Bernhardt, S. Wah Yee, C. Simons, M.-P. Lézé, R. W. Hartmann, A. Mularoni, G. Le Baut, I. Krimm, R. Abagyan, P. Le Pape and M. Le Borgne, *Pharmaceuticals*, 2020, **13**, 186.
 - 20 B. Schulzeab and U. S. Schubert, *Chem. Soc. Rev.*, 2014, **43**, 2522–2571.
 - 21 M. Azam Rasool, P. P. Pescarmona and I. F. J. Vankelecom, *ACS Sustainable Chem. Eng.*, 2019, **7**, 13774–13785.
 - 22 K. Soga, Y. Tazuke, S. Hosoda and S. Ikeda, *J. Polym. Sci. Polym. Chem. Ed.*, 1977, **15**, 219–229.
 - 23 M. Huang, L. Gao, J. Feng, X. Huang, Z. Li, Z. Huang and Li Wang, *ACS Omega*, 2020, **5**, 17808–17817.
 - 24 K. A. Salmeia, S. Vagin, C. E. Anderson and B. Rieger, *Macromolecules*, 2012, **45**, 8604–8613.
 - 25 F. A. Cotton and G. Wilkinson, *Adv. Inorg. Chem.*, 4th ed. Wiley, New York, 1980; p 775.
 - 26 W. Kläui, *J. Chem. Soc., Chem. Commun.*, 1979, 700–700.
 - 27 P. Gütllich, B. R. McGarvey and W. Kläui, *Inorg. Chem.*, 1980, **19**, 3704–3706.
 - 28 G. Navon and W. Kläui, *Inorg. Chem.* 1984, **23**, 2722–2725.
 - 29 W. Kläui, W. Eberspach and P. Gütllich, *Inorg. Chem.*, 1987, **26**, 3977–3982.
 - 30 J. M. Stauber, S. Zhang, N. Gvozdik, Y. Jiang, L. Avena, K. J. Stevenson and C. C. Cummins, *J. Am. Chem. Soc.*, 2018, **140**, 538–541.
 - 31 E. D. McKenzie and J. M. Worthington, *Inorg. Chim. Acta* 1976, **16**, 9–15.
 - 32 D. T. Shay, G. P. A. Yap, L. N. Zakharov, A. L. Rheingold and K. H. Theopold, *Angew. Chem. Int. Ed.*, 2006, **45**, 7870–7870.
 - 33 E. R. King, G. T. Sazama and T. A. Betley, *J. Am. Chem. Soc.*, 2012, **134**, 17858–17861.
 - 34 P. O. Lagaditis, B. Schluschaß, S. Demeshko, C. Würtele and S. Schneider, *Inorg. Chem.*, 2016, **55**, 4529–4536.
 - 35 Y. Baek and T. A. Betley, *J. Am. Chem. Soc.*, 2019, **141**, 7797–7806.
 - 36 A. Reckziegel, C. Pietzonka, F. Kraus and C. G. Werncke, *Angew. Chem. Int. Ed.*, 2020, **59**, 8527–8531.
 - 37 R. Poli and J. N. Harvey, *Chem. Soc. Rev.*, 2003, **32**, 1–8.
 - 38 D. Schröder, S. Shaik and H. Schwarz, *Acc. Chem. Res.*, 2000, **33**, 139–145.
 - 39 S. E. Neale, D. A. Pantazis and S. A. Macgregor, *Dalton Trans.* 2020, **49**, 6478–6487.
 - 40 Y. Yu, G. Luo, J. Yang and Y. Luo, *Catal. Sci. Technol.*, 2019, **9**, 1879–1890.
 - 41 L. Chaussy, D. Hegebaum-Reignier, S. Humbel, P. Nava, *Phys. Chem. Chem. Phys.*, 2022, **24**, 21841–21852.
 - 42 Y. Zhao and D. G. A. Truhlar, *J. Chem. Phys.*, 2006, **125**, 194101.
 - 43 J. Tao, J. P. Perdew, V. N. Staroverov and G. E. Scuseria, *Phys. Rev. Lett.*, 2003, **91**, 146401.
 - 44 Y. Zhao and D. G. Truhlar, *Theor. Chem. Acc.*, 2008, **120**, 215–241.
 - 45 A. D. Becke, *J. Chem. Phys.*, 1993, **98**, 5648–5652.
 - 46 C. Lee, W. Yang and R. G. Parr, *Phys. Rev. B: Condens. Matter Mater. Phys.*, 1988, **37**, 785–789.
 - 47 J. Tao, J. P. Perdew, V. N. Staroverov and G. E. Scuseria, *Phys. Rev. Lett.*, 2003, **91**, 146401.
 - 48 V. N. Staroverov, G. E. Scuseria, J. Tao and J. P. Perdew, *J. Chem. Phys.*, 2003, **119**, 12129–12137.
 - 49 K. P. Jensen and J. Cirera, *J. Phys. Chem. A*, 2009, **113**, 10033–10039.
 - 50 K. Chen, H. Zhu, Y. Li, Q. Peng, Y. Guo and X. Wang, *ACS Catal.* 2021, **11**, 13696–13705.
 - 51 L. Hu and H. Chen, *ACS Catal.*, 2021, **11**, 4593–4605.
 - 52 J. Liu, Z. Wei and H. Jiao, *ACS Catal.*, 2021, **11**, 4593–4605.
 - 53 C.-S. Wang, Y. Yu, Y. Sunada, C. Wang and N. Yoshikai, *ACS Catal.*, 2022, **12**, 4054–4066.
 - 54 D. Decker, Z. Wei, J. Rabeah, H.-J. Drexler, A. Brückner, H. Jiao and T. Beweries, *Inorg. Chem. Front.*, 2022, **9**, 761–770.
 - 55 Y. Hirata, D. Sekine, Y. Kato, L. Lin, M. Kojima, T. Yoshino and S. Matsunaga, *Angew. Chem. Int. Ed.*, 2022, e20220534.
 - 56 M. J. González, F. Bauer and B. Breit, *Org. Lett.* 2021, **23**, 8199–8203.
 - 57 N. J. Britto and M. Jaccob, *J. Phys. Chem. A*, 2021, **125**, 9478–9488.
 - 58 C. C. Bories, M. Barbazanges, E. Derat and M. Petit, *ACS Catal.*, 2021, **11**, 14262–14273.
 - 59 A. V. Marenich, C. J. Cramer and D. G. Truhlar, *J. Phys. Chem. B*, 2009, **113**, 18, 6378–6396.
 - 60 S. A. Frith and J. L. Spencer, *Inorg. Synth.*, 1990, **28**, 273–279.
 - 61 a) benzoyl fluoride: A. L’Heureux, F. Beaulieu, C. Bennett, D. R. Bill, S. Clayton, F. LaFlamme, M. Mirmehrabi, S. Tadayon, D. Tovell and M. Couturier, *J. Org. Chem.*, 2010, **75**, 3401–3411; b) 4-chlorobenzoyl fluoride: T. Scattolin, K. Deckers and F. Schoenebeck, *Org. Lett.*, 2017, **19**, 5740–5743; c) 4-methoxybenzoyl fluoride: M. Arisawa, Y. Igarashi, H. Kobayashi, T. Yamada, K. Bando, T. Ichikawa and M. Yamaguchi, *Tetrahedron*, 2011, **67**, 7846–7859; d) 4-nitrobenzoyl fluoride: ref 15; e) 1-fluorooctane: H. Koroniak, J. Walkowiak, K. Grys, A. Rajchel, A. Alty, R. Du Boisson, *J. Fluor. Chem.*, 2006, **127**, 1245–1251; f) Benzyl fluoride: P. Xu, F. Wang, G. Fan, X. Xu and P. Tang, *Angew. Chem. Int. Ed.*, 2017, **56**, 1101–1104; Fluoroacetamide: NMR spectra are available from commercial sources.
 - 62 M. J. Frisch, G. W. Trucks, H. B. Schlegel, G. E. Scuseria, M. A. Robb, J. R. Cheeseman, G. Scalmani, V. Barone, B. Mennucci, G. A. Petersson, H. Nakatsuji, M. Caricato, X. Li, H. P. Hratchian, A. F. Izmaylov, J. Bloino, G. Zheng, J. L. Sonnenberg, M. Hada, M. Ehara, K. Toyota, R. Fukuda, J. Hasegawa, M. Ishida, T. Nakajima, Y. Honda, O. Kitao, H. Nakai, T. Vreven Jr., J. A. Montgomery, J. E. Peralta, F. Ogliaro, M. Bearpark, J. J. Heyd, E. Brothers, K. N. Kudin, V. N. Staroverov, R. Kobayashi, J. Normand, K. Raghavachari, A. Rendell, J. C. Burant, S. S. Iyengar, J. Tomasi, M. Cossi, N. Rega, J. M. Millam, M. Klene, J. E. Knox, J. B. Cross, V. Bakken, C. Adamo, J. Jaramillo, R. Gomperts, R. E. Stratmann, O. Yazyev, A. J. Austin, R. Cammi, C. Pomelli, J. W. Ochterski, R. L. Martin, K. Morokuma, V. G. Zakrzewski, G. A. Voth, P. Salvador, J. J. Dannenberg, S. Dapprich, A. D. Daniels, Ö. Farkas, J. B. Foresman, J. V. Ortiz and J. Cioslowski, D. J. Fox, Gaussian 09, revision D.01; Gaussian, Inc.; Wallingford CT, 2009.
 - 63 F. Weigend and R. Ahlrichs, *Phys. Chem. Chem. Phys.*, 2005, **7**, 3297–3305.

- 64 S. Grimme, J. Antony, S. Ehrlich and H. Krieg, *J. Chem. Phys.*, 2010, **132**, 154104.
- 65 E. R. Johnson and A. D. A. Becke, *J. Chem. Phys.*, 2005, **123**, 024101.
- 66 G. Scalmani, M. J. Frisch, *J. Chem. Phys.*, 2010, **132**, 114110.
- 67 CYLview, 1.0b, C. Y. Legault, Université de Sherbrooke, 2009.
<http://www.cylview.org/>
- 68 *SAINT+*: Area-Detector Integration Software, version 6.01; Bruker AXS: Madison, WI, 2001.
- 69 G. M. Sheldrick, *SADABS program*; University of Göttingen: Göttingen, Germany, 1999.
- 70 G. M. Sheldrick, *SHELXS 97, Program for the Solution of Crystal Structure*; University of Göttingen: Göttingen, Germany, 1997.
- 71 G. M. Sheldrick, *Acta Cryst., Sect. C: Struct. Chem.*, 2015, **71**, 3–8.
- 72 L. J. Farrugia, *J. Appl. Cryst.*, 2012, **45**, 849–854.